01 Aug 2022

Huber Kalman Filter for Wi-Fi based Vehicle Driver's Respiration Detection

Yang Yang

Yunlong Luo

Alex Qi

Ge Shi

et. al. For a complete list of authors, see https://scholarsmine.mst.edu/ele_comeng_facwork/4635

Recommended Citation

Y. Yang et al., "Huber Kalman Filter for Wi-Fi based Vehicle Driver's Respiration Detection," *IEEE Transactions on Vehicular Technology*, vol. 71, no. 8, pp. 8933 - 8943, Institute of Electrical and Electronics Engineers, Aug 2022.
The definitive version is available at https://doi.org/10.1109/TVT.2022.3174819

Huber Kalman Filter for Wi-Fi Based Vehicle Driver's Respiration Detection

Yang Yang, *Student Member, IEEE*, Yunlong Luo, *Student Member, IEEE*, Alex Qi, *Member, IEEE*, Ge Shi, *Member, IEEE*, Miao Miao, *Member, IEEE*, Jun Fan, *Fellow, IEEE*, Jianhua Ma, *Senior Member, IEEE*, and Yihong Qi, *Senior Member, IEEE*

***Abstract*—The use of breath detection in vehicles can reduce the number of vehicular accidents caused by drivers in poor physical condition. Prior studies of contactless respiration detection mainly targeted a static person. However, there are emerging applications to sense a driver, with emphasis on contactless methods. For example, being able to detect a driver's respiration while driving by using a vehicular Wi-Fi system can significantly enhance driving safety. The sensing system can be mounted on the back of the driver's seat, and it can sense the tiny chest displacement of the driver via Wi-Fi signals. The body displacement and car vibrations could introduce significant noise in the sensed signal. The noise then needs to be filtered to obtain the driver's respiration. In this work, the noise in the sensed signal is proposed to be reduced using a Huber Kalman filter to restore the original respiration curve. Through several experiments in terms of different drivers, different car models, multiple passengers, and abnormal breathing, we demonstrate the accuracy and robustness of the Huber Kalman filter in driver's respiration.**

***Index Terms*—Huber Kalman filter, respiration detection for the driver, the noisy sensing signal, vehicular Wi-Fi sensing, wireless sensing.**

I. Introduction

With the increase of the total number of vehicles, the incidence of traffic accidents also increases, and the society attaches great importance to driving safety. According to the Road Traffic Injuries report released by the World Health Organization (WHO) in 2021, road traffic crashes result in the deaths of approximately 1.3 million people around the world each year, with one of the important risk factors as fatigue driving [1]. Such car accidents could be effectively avoided, and human lives could be saved if drivers are warned when they become sleepy or impaired physically [2]. Drowsy driving can be indicated by multiple symptoms of the driver, such as eyelid movements, driving movements, and human vital signs, among which, respiratory rate is a valuable indicator of driver fatigue status. Research shows that the breathing rate usually drops significantly (about three breaths per minute (bpm)) before the driver falls asleep [2]–[3]. Thus, accurate monitoring of the driver's breathing rate will help prevent the occurrence of drowsy driving. Further research into respiration waveform analysis and respiration rate variability (RRV) could help reduce false positives [4]. Therefore, monitoring to obtain a true respiratory waveform is necessary.

Different techniques have been proposed for respiration monitoring by using various sensing devices, including contact-based respiration belt to detect thoracic rise and fall [5], acoustic-based [6], vision-based ones used in video cameras [7]–[8], and the radio frequency-based (RF) ones [9]–[15]. A contact respiration belt is inconvenient and uncomfortable to wear on the chest or abdominal area. Xu *et al.* proposed a fine-grained breathing monitoring system, Breath-Listener, which utilizes an acoustic device on a smartphone to estimate fine-grained breathing waveform in driving environments [6]. But when other passengers are in the car, especially seated in the front passenger seat, it can interfere with the driver's breath detection. The vision-based method is to detect respiration by analyzing the chest movements captured by a video camera [7]. Still, it may not work well when the lighting condition is poor (e.g., driving at night) and it may raise privacy concerns. Among the RF based methods, with the vigorous deployment of Wi-Fi and the popularization of intelligence terminals, respiration detection using the existing Wi-Fi is widely studied [16]–[18]. With the development of the mobile Internet, the Internet of Vehicles, and the Internet of Things, an era of smart cars is coming. By carrying onboard Wi-Fi products, users can enjoy ubiquitous information services. In-vehicle Wi-Fi has become standard on many new models. For the driver's breath detection, it is easy to deploy at a low cost by using the existing in-vehicle Wi-Fi equipment to realize the integration of communication and sensing [17]. Moreover, compared with other high-frequency wireless sensors, Wi-Fi has less penetration loss and can be installed on the back of the driver's seat. Compared to the front, side, and top mounting, the benefit is to avoid the distraction of arms turning the steering

Manuscript received 21 August 2021; revised 10 April 2022; accepted 9 May 2022. Date of publication 25 May 2022; date of current version 15 August 2022. The review of this article was coordinated by Prof Linke Guo. *(Corresponding author: Yihong Qi.)*

Yang Yang and Yunlong Luo are with the School of Information Science and Technology, Southwest Jiaotong University, Chengdu 611756, China (e-mail: yang0206@my.swjtu.edu.cn; yunlong.luo@my.swjtu.edu.cn).

Alex Qi and Ge Shi are with the Pontosense Inc, Kitchener N2H5G5, Canada (e-mail: alex.qi@pontosense.com; ge.shi@mercku.com).

Miao Miao is with the Gingko College of Hospitality Management, Chengdu 611743, China (e-mail: miaomiao8084@gmail.com).

Jun Fan is with the Missouri University of Science and Technology, Rolla 65409 USA (e-mail: jun.fan@ieee.org).

Jianhua Ma is with the Hosei University, Chiyoda City, Tokyo 102-8160, Japan (e-mail: jianhua@hosei.ac.jp).

Yihong Qi is with the Pontosense Inc, Kitchener N2H5G5, Canada, with the Southwest Jiaotong University, Chengdu 611756, China, and also with the Missouri University of Science and Technology, Rolla 65409 USA (e-mail: yihong.qi@dbjtech.com).

Digital Object Identifier 10.1109/TVT.2022.3174819

wheel and the distraction of other passengers. Therefore, the Wi-Fi based breath detection is an attractive solution for smart vehicles. Many scholars have conducted extensive studies on Wi-Fi based respiration detection. In [13], it illustrates the first to utilize the CSI phase difference data to remotely detect breathing and heart rates with commodity Wi-Fi devices. Wang *et al.* first provided a rigorous analysis of the CSI phase difference data with respect to its stability and periodicity. In [19], the study only focuses on detecting passenger breathing, which should be utterly static after the vehicle is parked, to see the unsupervised child left in the car. While these methods work fine under controlled environments and conditions for stationary people, several challenges need to be addressed to make these systems reliable and robust enough to withstand the impact of body movement in a moving car under different road types of traffic conditions.

Compared with the conventional stationary applications of Wi-Fi based respiration detection, the vehicle application scenarios are quite different and challenging when the vehicle is in motion. The received signal includes the driver's breathing motion that we would like to detect modulated by the unwanted motion induced by different driving conditions. Different driving conditions, including engine vibration, braking and acceleration on the road, result in various degrees of driver body displacement. During driving, the breathing curve of the driver will be affected by three prominent noises: 1) body movements when controlling the steering wheel during driving; 2) body displacement associated with driving conditions, such as body position relative to the sensor changes when braking, accelerating, and turning; 3) the mechanical changes in the car seat when the engine vibrates, and deformation under different pressures of the driver. The body movements and the body displacement bring "large" errors. And the third case above brings "small" errors.

For the above problems, Cruz *et al.* [20] introduced a mathematical framework. They proposed to attach an accelerometer to the radar-based sensor to record the acceleration of movement due to unnecessary external influences. After subtracting this part of the motion, the radar signal only contains the characteristics of breathing movement. But they assumed a constant vehicle velocity and a simplified "rigid human" model. Kalman filtering is an essential data processing method used to estimate the actual value in the presence of interference [21], it can be used to effectively reduce measurement error and random noise in the system [22]–[24]. However, when there is a large data error, Kalman filter performance is limited. When the Kalman filter calculates the Kalman gain, it uses the second norm, which is greatly affected by outliers. As a result, the Kalman filter cannot deal with large error points. However, the Huber function offers a good balance when dealing with large data errors and small uncertainties [25]. In this paper, a new filtering algorithm is proposed, which improves the iterative process of the Kalman filtering by using a Huber objective function. Combining the advantages of the Kalman filter and the Huber objective function can filter out large errors and small fluctuations quickly and effectively and provide smoother and less biased estimation results.

Overall, this paper introduces an accurate and robust respiration detection system for in-vehicle scenarios. In particular, the system utilizes the Kalman filter based on the Huber function to estimate the breathing waveform during driving. This paper is divided into five parts. Section II briefly introduces the structure of a prototype for a Wi-Fi-based vehicular respiration detection system and a principle of respiration detection. Section III describes the proposed Huber Kalman filtering method. Section IV shows the performance of the algorithm verified by experiments. Finally, the summary and discussions are included in the last section.

II. Wi-Fi Based Vehicular Respiration Detection System

A Wi-Fi based respiration detection system suitable for vehicular applications is presented below. As shown in Fig. 1(a), the system generates the wireless signal, divided into two identical signals through a power splitter. One is directly connected to the receiver RX1 through a coaxial cable, serving as a reference signal. The other is transmitted through space, reflected by the driver's chest, and received by the receiver RX2.

The system analyzes the change of the phase difference between the two received Channel State Information (CSI) signals at RX1 and RX2. The distance between the received antenna and the driver's chest changes periodically due to the fluctuation of the chest during the driver's breathing. Therefore, the difference between the propagation paths of the two received signals changes accordingly. The changes in the phase and the path differences are related as:

$$\Delta\phi\ (t) = \frac{2\pi\Delta d\,(t)}{\lambda} \tag{1}$$

Where $\Delta \mathrm{d}(\mathrm{t})$ and $\Delta\phi(t)$ are the changes of the path and phase difference between the two received signals, respectively; and λ is the wavelength. In other words, the change in the phase difference contains information about the driver's chest displacement. To achieve the functions described above, the system is implemented in three parts: data collection, data preprocessing, and data analysis, with the block diagram shown in Fig. 1(b).

A. Data Collection

Orthogonal Frequency Division Multiplexing (OFDM) is widely used in modern wireless network standards, such as Wi-Fi (i.e., IEEE 802.11a/g/n) [13], [15], [26]. OFDM divides the spectrum into multiple orthogonalized subcarriers on which wireless data is transmitted. Leveraging the device driver for off-the-shelf NICs, e.g., the IPQ4019, we can extract the CSI from the NIC, which is fine-grained physical layer (PHY) information. CSI reveals the channel characteristics experienced by the received signal such as the multipath effect, shadow fading, and distortion.

With OFDM, the Wi-Fi channel at the 5 GHz band can be considered as a narrowband flat fading channel. In the frequency domain, the channel model can be expressed as $\vec{Y} = CSI \cdot \vec{X} + \vec{N}$, where $\vec{Y}$ and $\vec{X}$ denote the received and transmitted signal vectors, respectively, $\vec{N}$ is the additive white Gaussian noise, and CSI represents the channel's frequency response, which can be estimated from $\vec{Y}$ and $\vec{X}$ [13].

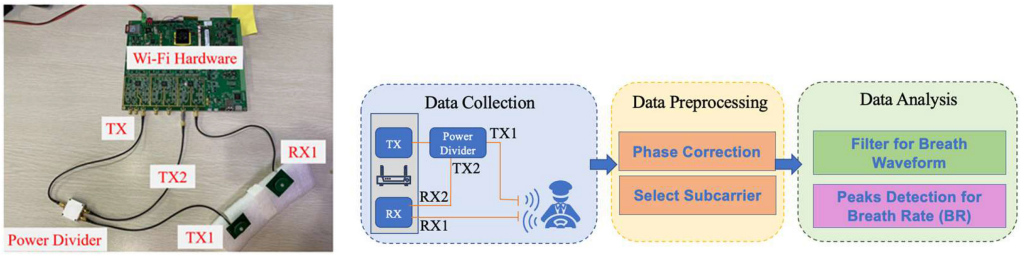

Fig. 1. (a) Wi-Fi device. (b) Block diagram of the prototype respiration detection system for vehicular applications.

The channel frequency response of subcarrier i, CSI_i, is a complex value. That is

$$CSI_i = I_i + j\, Q_i = |CSI_i| \, \exp\left(j \angle CSI_i\right) \tag{2}$$

where I_i and Q_i are the in-phase component and quadrature component of subcarrier i, respectively; $|CSI_i|$ and $\angle CSI_i$ are the amplitude response and phase response of subcarrier i, respectively.

Let $\widehat{\angle CSI_i}$ denote the measured phase subcarrier i [13], which can be expressed as:

$$\widehat{\angle CSI_i} = \angle CSI_i + (\lambda_p + \lambda_s)\, m_i + \lambda_c + \beta + Z \tag{3}$$

where $\angle CSI_i$ is the true phase value, m_i is the subcarrier index of subcarrier i , β is the initial phase offset due to the phase-locked loop (PLL). Z is the measurement noise that is assumed to be AWGN of variance σ^2, and $\lambda_p, \lambda_s,\ \lambda_c$ are the phase errors from the packet boundary detection (PBD), the sampling frequency offset (SFO), and central frequency offset (CFO) respectively.

Note that RX1 and RX2 use the same clock and the same down-converter frequency. Consequently, the measured phases of subcarrier i from two antennas have identical packet detection delay, sampling periods, frequency differences, and the same index m_i. Thus, the measured phase difference on subcarrier i between two antennas can be approximated as

$$\widehat{\Delta\angle CSI_i} = \Delta\angle CSI_i + \Delta\beta + \Delta Z \tag{4}$$

where $\Delta\angle CSI_i$ is the true phase difference of subcarrier i, $\Delta\beta$ is the unknown difference in phase offsets, in fact a constant, and ΔZ is the noise difference with variance $2\sigma^2$.

As mentioned above, the phase information can be obtained by IQ demodulation. And the tiny displacement of the chest during breathing could be captured through the phase information of vehicular Wi-Fi. Theoretically, one received signal is sufficient as long as its phase information is accurately obtained. However, in reality, the IQ demodulation of a received CSI signal does not provide reliable phase information. This issue is resolved by providing a synchronized reference signal. Since the phase is a relative quantity, the phase difference between the received signal and the reference signal is the practical relative phase, which is reliable from the IQ demodulation.

B. Data Preprocessing

1) Phase Correction: The most common way to demodulate phase by IQ is arctangent demodulation. The value range of the phase resolved by CSI is $[-\pi, \pi]$. To maintain the simple relationship in (1), the measured CSI phase difference needs to be unwrapped before it can be used to calculate the chest movement.

The phase correction is accomplished as below [29], as long as the sample step is small enough such that the absolute value of the change of the measured phase difference between two neighboring sampling points is smaller than π. Then,

When $\Delta\phi_{n+1}\langle 0$ and $\Delta\phi_n\rangle 0$ as illustrated in Fig. 2(a), $\Delta\phi_{n+1}$ is corrected by adding 2π to its measured value.

When $\Delta\phi_{n+1} > 0$ and $\Delta\phi_n < 0$ as illustrated in Fig. 2(b), $\Delta\phi_{n+1}$ is corrected by subtracting 2π from its measured value.

The extracted phase sequence of breathing (phase difference between the two paths) is shown in Fig. 2(c), and Fig. 2(d) the corrected phase sequence of Fig. 2(c).

2) Subcarrier Selection: There are 53 subcarriers for Wi-Fi signals, and different subcarriers have different frequency bands. The noise levels for different subcarriers are also different [15]. For example, Fig. 3 shows 4 CSI phase difference data from Sub-Carriers #10, #20, #30, #40.

Therefore, the selection of subcarriers is necessary. In data preprocessing, several subcarrier groups with good quality need to be selected. Wang *et al.* proposed to use the mean absolute deviation of the CSI phase difference data from every subcarrier to quantify its sensitivity [13]. Generally, the larger the mean absolute deviation, the higher the sensitivity. Therefore, several larger groups can be selected by calculating the absolute deviation values of all the subcarriers. Liu, *et al.* revealed that the chest displacement due to breathing was cyclical [15]. If a CSI phase difference sequence can be accurately modeled as a sinusoidal wave, we regard it as high periodicity level. A subcarrier with a better periodicity was selected by quantifying the periodicity of the CSI phase difference data of each subcarrier. The work in this paper combines the two criteria proposed in the two reference papers and considers both the periodicity and the mean absolute deviation.

To quantify the periodicity of a phase sequence, we first model the sequence as a sinusoidal wave. Then the ratio of the two parameters, the amplitude of the sinusoid, and the goodness of fit of the sinusoid, is utilized to calculate the periodicity level [18], [27].

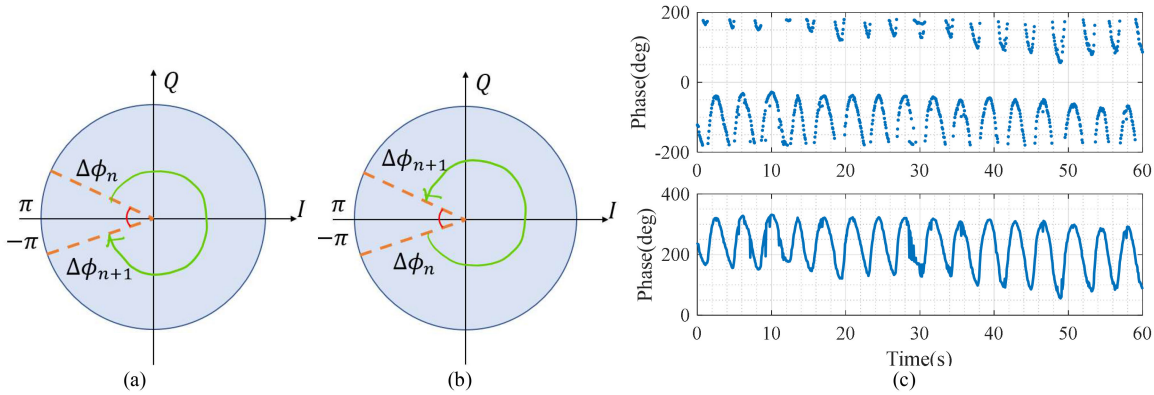

Fig. 2. Unwrapping the measured phase difference: (a) the increase of the measured phase difference from the nth step to the (n+1)th step is less than -π, (b) the decrease of the measured phase difference from the nth step to the (n+1)th step is greater than π, (c) the raw phase of breathing and the corrected phase after unwrapping.

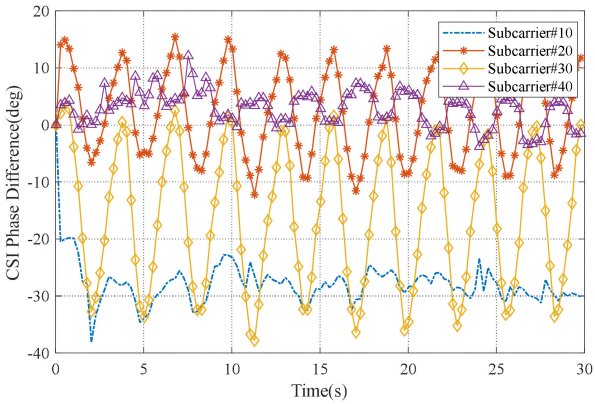

Fig. 3. Respiration curves captured by different subcarriers.

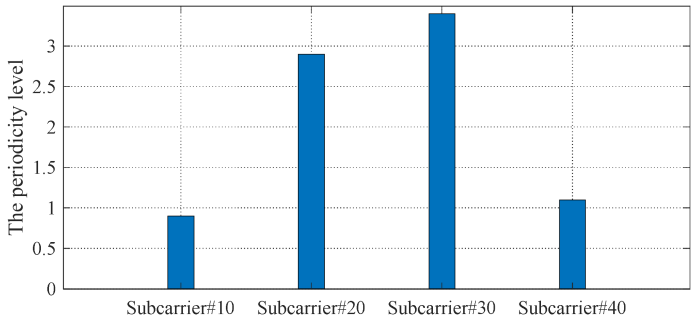

Fig. 4. The periodicity levels of different subcarriers.

When a person is breathing, a measured phase sequence $x(t)$ can be largely modelled as a sinusoidal wave:

$$x\ (t) = \ Asin\left(2\pi ft + \varphi\right) + D + \varepsilon\left(t\right) \tag{5}$$

where the constants A, f, φ and D are the amplitude, frequency, phase, and shift of the identified sinusoidal wave, and $\varepsilon(t)$ is an additive noise.

Given $x(t)$, the parameters of the sinusoidal wave (A, f, φ and D) can be identified using the Nelder-Mead method [28], which is a common non-linear optimization technique for multidimensional unconstrained minimization. Since the frequency f has already been estimated using the process described in [18], we regard f as a known constant when applying the Nelder-Mead method.

The goodness of fit can be calculated by the root-mean-square error (RMSE) defined as

$$RMSE\ = \sqrt{\frac{\sum_{t=1}^{n}\left(\hat{x}\left(t\right) - x\left(t\right)\right)^2}{N}} \tag{6}$$

where $\hat{x}(t)$ is the predicted values at time t using the sinusoidal model and n is the length of $x(t)$. Based on the RMSE and A, we define the periodicity level of $x(t)$, denoted as Pr, as the ratio of the two parameters:

$$Pr\ = \frac{A}{RMSE} \tag{7}$$

After calculating the above algorithm, Sub-Carriers #30 was selected as the best subcarrier, as shown in Fig. 4.

C. Data Analysis

For the static person under a controlled environment, a simple bandpass filter works well to restore the breathing waveform. Compared with the conventional stationary applications of Wi-Fi based respiration detection, the vehicle application scenarios are quite different and challenging when the vehicle is in motion. During driving, the acquired phase waveform includes four parts: 1) displacement of breathing; 2) body movements when controlling the steering wheel during driving; 3) body displacement associated with driving conditions, such as body position relative to the sensor changes when braking, accelerating, and turning; 4) the mechanical changes in the car seat when the engine vibrates, and deformation under different pressures of the driver. The noise and interference that do not belong to the driver's breathing need to be filtered out through the filter. And then after peak detection, all peak-to-peak intervals (PPI) are averaged to obtain the period of the breathing signal, denoted as P. Finally, the estimated breathing rate can be computed as 60/P bpm.

III. Breathing Estimation During Driving

A. Kalman Filters for Breathing Estimation

The Kalman filter is real-time, accurate and fast, and it is a powerful data processing tool that can effectively reduce measurement errors and deal with random noise in the system [22], [30]. Kalman filtering is often used in distance-velocity-acceleration based position tracking models. So similarly, the Kalman filter can also be used for a phase tracking model based on phase - angular velocity - angular acceleration.

We choose the phase ϕ_k and the angular frequency ω_k as our state variables [20]. The state uncertainty depends on (but is not equal to) the unknown acceleration $\dot{\omega}_{k-1}$. So, we can quickly obtain the following state-space description of the system:

$$x_k = \begin{pmatrix} \phi_k \\ \omega_k \end{pmatrix} \approx \begin{pmatrix} 1 & \Delta t \\ 0 & 1 \end{pmatrix} \begin{pmatrix} \phi_{k-1} \\ \omega_{k-1} \end{pmatrix} + \dot{\omega}_{k-1} \begin{pmatrix} 1/2\Delta t^2 \\ \Delta t \end{pmatrix} \quad (8)$$

The internal state of the process is considered unknown but can be estimated by measurements. Therefore, we must introduce a vector of measurement values and define their relationship to the state variables which can be done by defining:

$$z_k = \phi_k + v_k \quad (9)$$

where v_k describes the measurement noise and $p(v) \sim N(0, R)$.

A Kalman filter uses the last estimated state and the current measurement to assess the current state by calculating a weighted mean of the two. The Kalman Filter continuously calculates "optimal" weights (called Kalman filter gain coefficients) for optimum estimation accuracy or noise cancellation. This efficient and computable method can estimate the process state and minimize the mean square error of the estimation. The Kalman filter uses the feedback control method to assess the process state: the filter estimates the state of the process first, and then the feedback is obtained by measuring the variables. Therefore, the Kalman filter can be divided into the time updating equation and the measurement updating equation. The time updating equation predicts the prior state estimate of the next moment through historical data and the state transfer equation. And the measurement updating equation is responsible for correction. According to the combination of the prior estimate and the measurement, an improved posterior state estimate is constructed [31]. The established Kalman filter thus has the prediction-update model shown in Fig. 5 [31].

Define P_k as the error covariance, expressed as

$$P_k = E\left[e_k e_k^T\right] \quad (10)$$

The estimation principle of the Kalman filter is to minimize the covariance of the optimal state estimation P_k, making it closer to the actual value. Therefore, its objective function is:

$$J = \min \sum P_k \quad (11)$$

It can be seen from this formula that the Kalman filter is based on the estimation of the second norm. The second norm is greatly affected by outliers, so the result of the Kalman filter is affected by large error points. Compared with the second norm, the first norm has better robustness for large errors, but when small fluctuations, its optimization results are biased to some subsets of the data. Neither the first norm nor the second norm can effectively treat all the errors. Fortunately, the Huber function offers a good balance when dealing with large errors and small uncertainties [25]. It integrates the advantages of the first norm and the second norm and applies the first norm when handling a large error and the second norm when dealing with a small fluctuation for evaluation. In this paper, we propose to use the Huber function as the objective function in the Kalman filter, resulting in a novel Huber Kalman filter, for the Wi-Fi based respiration detection in-vehicle environments.

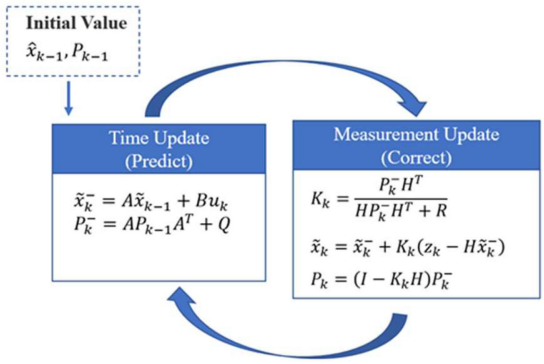

Fig. 5. Kalman filter prediction-update model.

B. Huber Kalman Filters for Breathing Estimation

1) Characteristics of Huber Objective Function: As mentioned earlier, in the common least square method, the second norm ℓ_1 is easily affected by large errors. On the contrary, the first norm ℓ_1 has good robustness against large error, but when there are small fluctuation errors in the data, the ℓ_1-based solution is often biased to a subset of the data. In 1993, J.W. Bandler [25] proposed the Huber objective function in the common least square method combining the first norm and the second norm functions, taking advantage of the two to provide smoother and less biased estimates. The Huber objective function is defined as follows:

$$\rho_a(f) = \begin{cases} \frac{f^2}{2} & \text{if } f \le a \\ a|f| - \frac{a^2}{2} & \text{if } f > a \end{cases} \quad (12)$$

where a is a positive constant to define the threshold between the large and small errors, and f is the error function. The proportion of processing error functions in ℓ_1 or ℓ_2 can be changed by changing a. When a is large enough, the optimization problem becomes the conventional least square problem. When a approaches 0, the optimization problem becomes the first norm based one. As shown in Fig. 6, the definition of ρ_a ensures a stationary transition at $|f| = a$, i.e., the first derivative of the Huber objective function is continuous.

2) Huber Kalman Filter: To resolve the issue in the conventional Kalman filter, in this paper, we propose to use the Huber function as the objective function in the Kalman filter, leading to a novel Huber Kalman filter.

The prior estimation error and the posteriori estimation error are represented as e_k^- and e_k, which represent the difference

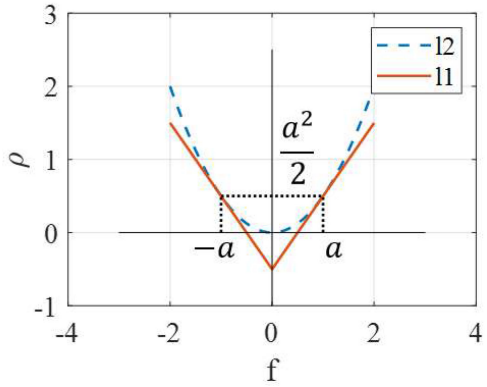

Fig. 6. Huber objective function.

between the prior estimate $\tilde{x}_k^-$, the best estimate $\tilde{x}_k$ and the true value x_k, respectively. The covariances of the prior estimation error and the posterior estimation error are as follows piecewise function:

$$P_k^- = \begin{cases} \frac{e_k^{-2}}{2} & \text{if } \left|e_k^-\right| \le a \\ a\left|e_k^-\right| - \frac{a^2}{2} & \text{if } \left|e_k^-\right| > a \end{cases} \tag{13}$$

$$P_k = \begin{cases} \frac{e_k^2}{2} & \text{if } |e_k| \le a \\ a\,|e_k| - \frac{a^2}{2} & \text{if } |e_k| > a \end{cases} \tag{14}$$

Combined $\tilde{x}_k = \tilde{x}_k^- + K_k(z_k - H\tilde{x}_k^-)$, P_k represented by P_k^- as

$$P_k = \begin{cases} \frac{(I-KH)P_k^-(I-KH)^T + KRK^T}{2} & \text{if } 0 \le P_k^- \le \frac{a^2}{2} \\ (I-KH)\left(P_k^- + \frac{a^2}{2}\right) - \frac{a^2}{2} & \text{if } P_k^- > \frac{a^2}{2} \end{cases} \tag{15}$$

The estimation principle of the Kalman filter is to minimize the error function of the optimal state estimation to approach the true value. Therefore, the objective function is modified as formula (11).

Taking the partial derivative of (15) for the Kalman gain coefficient *K* results in:

$$\frac{\partial P_k}{\partial K_k} = \begin{cases} -P_k^- H^T + K\left(HP_k^- H^T + R\right) \\ \text{if } 0 \le P_k^- \le \frac{a^2}{2} \\ \frac{HK_kH^T - H}{|1-K_kH|}\left(P_k^- + \frac{a^2}{2}\right) \\ \text{if } P_k^- > \frac{a^2}{2} \end{cases} \tag{16}$$

By setting the partial derivative in (16) to 0, we obtain

$$K_k = \begin{cases} \frac{P_k^- H^T}{HP_k^- H^T + R} & \text{if } 0 \le \mathrm{P_k^-} \le \frac{a^2}{2} \\ \frac{1}{H} & \text{if } \mathrm{P_k^-} > \frac{a^2}{2} \end{cases} \tag{17}$$

It's easy to derive that P_k^- is represented by P_k as follows:

$$P_k^- = \begin{cases} \frac{AP_{k-1}A^T + Q}{2} & \text{if } 0 \le \mathrm{P_{k-1}} \le \frac{a^2}{2} \\ |A|\left(P_{k-1} + \frac{a^2}{2}\right) - \frac{a^2}{2} & \text{if } \mathrm{P_{k-1}} > \frac{a^2}{2} \end{cases} \tag{18}$$

With all these, the time updating and state updating equations based on the Huber objective functions can be derived as Fig. 7.

3) Parameter a: As shown in the (12) and Fig. 6, the Huber function is a hybrid of the least-squares ℓ_2 (when $|f| \le a$) and ℓ_1 (when $|f| > a$) functions. The ℓ_1 is robust against gross errors. Since the Huber function treats errors above threshold in the ℓ_1 sense, it is robust against those errors, the solution is not sensitive to those errors. The choice of a defines the threshold between "large" and "small" errors. By varying a, we can alter the pro-portion of error functions to be treated in the ℓ_1 and ℓ_2 sense [25].

We can also define N_s as the number of "small errors". The cardinality of the set refers to all number of errors, defined as N. Fig. 8(d) depicts N_s versus a, where ordinate is expressed as a percentage of the number of "small errors" N_s and the total number of devices N. The turning point as shown in the Fig. 9, called "knee" on the curve by J. W. Bandler [25], which is consistent with the solution that includes a majority of functions as "small errors." The value of a at the "knee", which provides a clear line between the "large" and "small" errors, is consistent with our choice.

During initialization, there is a 20-second startup time. The P_k is recorded during the iteration. From P_k, we can get e_k. Adjusting a, there are different proportions of large error and small error. The value of a at the "knee" is set. In the real-time process, e_k in the past 20-second time window is continuously analyzed to set the value of a adaptively. During driving, different driving scenarios have different data characteristics and different error distributions. Therefore, different thresholds a should be selected for different scenarios. To illustrate Huber Kalman is dependent on the threshold a, we show the error distribution and the filtering results of different driving scenes in Fig. 8. When the engine is turned off, there are fewer errors, and more points are evaluated by the second norm. When the engine is turned on, some of the sampling points are now considered to be "large" errors and the remaining are considered "small" errors. Therefore, they use the first norm and the second norm, respectively.

4) Data Analysis: Fig. 9 is a breath wave of the driver during driving. As shown in Table I, the error of the original phase after the Kalman filtering is 1 beat/min, and the error after the Huber Kalman filtering is 0 beat/min. The errors of the average peak-to-peak interval after the Kalman filtering and the Huber Kalman filtering are 110 s and 45 s, and the correlation coefficients of the waveforms after the Kalman filtering and the Huber Kalman filtering are 0.8293 and 0.9156, respectively. These results clearly demonstrate that, in the driving situation, the Huber Kalman filter is more suitable for dealing with large and small errors, and the recovered breathing waveform correlates well with that from the reference device. The better correlation in peak-to-peak

TABLE I
THE RESULT OF DIFFERENT FILTERS

Methods	BR errors (bpm)	PPI errors (ms)	Corr_Coeff
BPF	2	346	0.768
KF	1	110	0.8293
HKF	0	45	0.9156

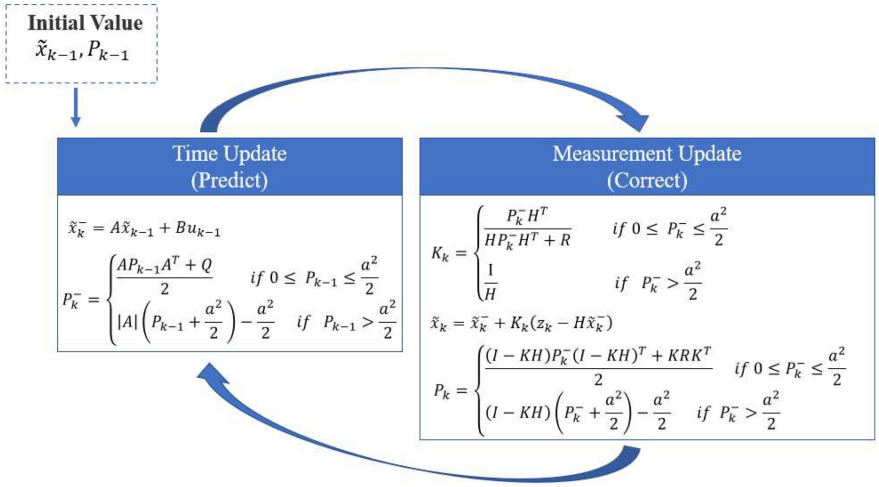

Fig. 7. Huber Kalman filter prediction-update model.

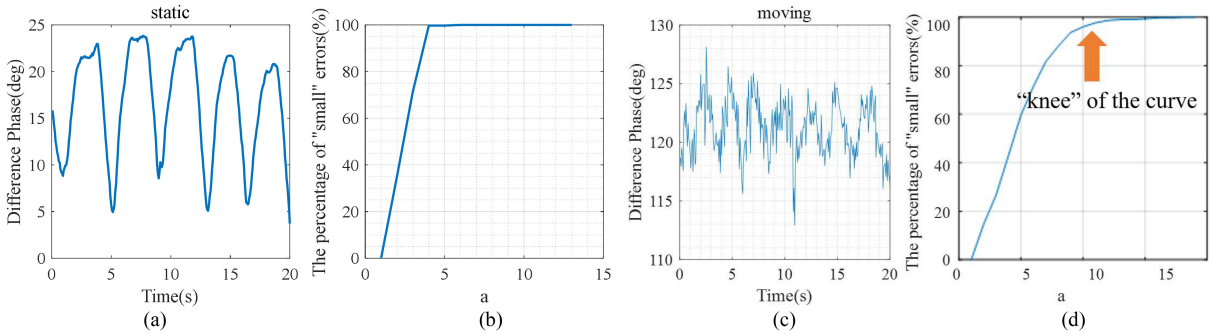

Fig. 8. (a) Raw data of respiration when the engine is not started; (b) The value of threshold value a in scenario(a) is the "knee" of the curve; (c) Raw data of respiration when the engine is working; (d) The value of threshold value a in scenario(c) is the "knee" of the curve.

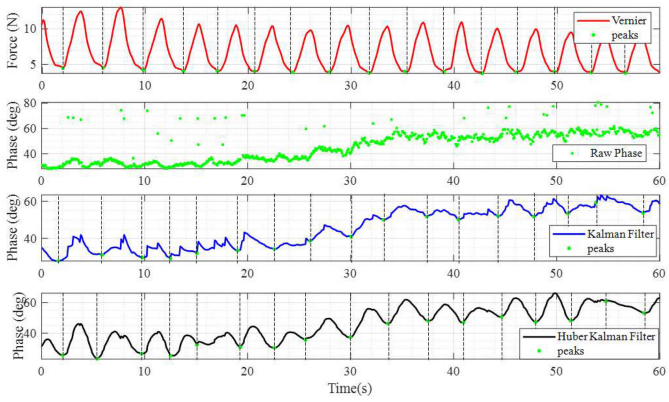

Fig. 9. Comparison of Kalman filtering and Huber Kalman while driving.

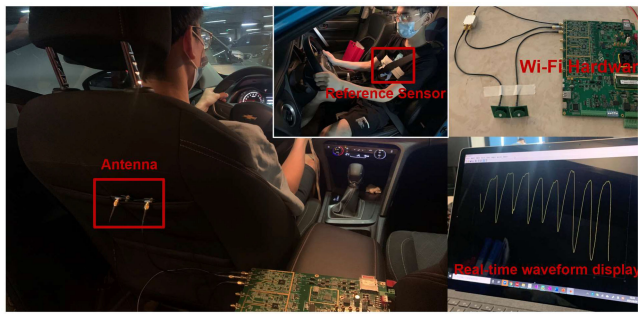

Fig. 10. Experimental setup of the proposed system for Wi-Fi-based breathing detection.

interval of the Huber Kalman filtering can be further used for impaired or fatigue driving research and applications.

IV. Experimental Results

A. Experimental Environment

The proposed respiration detection system based on the Wi-Fi was then used to detect the respiration of the driver. The sensor was mounted on the back of the seat, the signal passed through the seat and reflected from driver's back, which can avoid complex reflections due to multiple people and avoid the influence of the arms that turn the steering wheel while driving. As shown in Fig. 10, the system was arranged behind the driver's seat at the approximate location of the chest, with the antenna facing the driver's back. To validate the effectiveness of the Wi-Fi based vital sign detection, the driver also wore a wearable sensor, a Vernier Respiration Belt, for breath monitoring used as the reference for comparison. The respiration belt uses a force sensor and an adjustable nylon strap around the chest to measure respiration effort and respiration rate. During driving, the detection result of the wearable device is almost unaffected

by the driving conditions. Each experiment covers a variety of driving scenarios, like starting, turning, speeding up, speeding down and stopping. Data of the experiments were collected and compared among different filtering cases and to the reference data, demonstrating the effectiveness of the proposed Huber Kalman filter for Wi-Fi based respiration detection in vehicles.

B. Experimental Method

In total, 8 participants (four males and four females) aging from 20 to 60 were invited to conduct experiments. We evaluated the overall performance of the Huber Kalman filter for different scenarios involving different drivers, different car models and multiple passengers. Both normal and abnormal breathing of drivers were included in the experiments. We compared the Huber Kalman filter and the Kalman filter with the common breath rate estimation technique using a bandpass filter. To evaluate the performance of different filters, we defined three metrics: Breath Rate Error, PPI Error, and Correlation Coefficient (Corr-Coeff) with a reference device.

- Breath Rate Error: The error of the estimated breath rate RE compared to the reference breathing rate RR, which is defined as the difference between RE and RR, i.e., (RE - RR).
- PPI Error: After peak detection, all peak-to-peak intervals (PPI) are averaged to obtain the period of the breathing signal, denoted as P. The error of the estimated P (PE) compared to the reference P (PR), which is defined as the difference between PE and PR, i.e., (PE - PR).
- Corr-Coeff: Corr-Coeff reflects the similarity of the estimated respiration waveform to the reference device. The correlation coefficient is between -1 and 1, and larger than 0.8 indicates a strong positive relationship.

C. Experimental Results

1) Overall Performance: We evaluated the overall performance of the proposed system for different drivers and for different breathing frequency ranges of drivers. Both normal and abnormal breathing of the driver were included in the assessment. Different car models and a variable number of passengers were involved as well. Each set of experiments is driven on the road for 2 minutes, during which driving scenarios such as acceleration, braking, and cornering may be encountered naturally. Overall, as shown in Fig. 11, the probability when the breathing rate error equals to 0 bpm after the Huber Kalman filter is 0.56, which is significantly higher than those after the bandpass filter and the Kalman filter. The breathing rate error of all test results was less than 3 bpm. As shown in Fig. 12, during driving, the average correlation coefficient between the time-domain waveform recovered by the Huber Kalman filter and the reference device reached 0.9, which means that the Huber Kalman filter almost recovered the true waveform.

2) Impact of Different Car Models: Fig. 13 shows the experimental results for 6 models labeled as A to F. The test results of model A are the best, with the average errors of the breath rate and the PPI as about 0.17 bpm and 20 ms, respectively, and the correlation coefficient as 0.9. The average breath rate error of

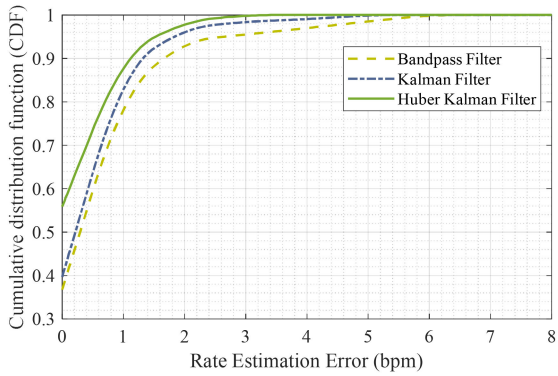

Fig. 11. CDF of overall breathing rate estimation error.

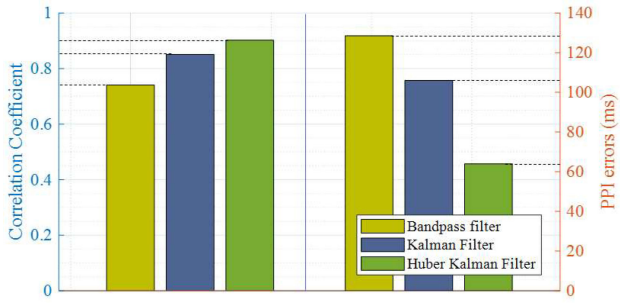

Fig. 12. Overall breathing correlation coefficient and PPI error.

the worst model C also reached 0.43 bpm, with the correlation coefficient as 0.88, which fully meets the requirements for respiration detection in the cabin.

3) Impact of Different Drivers: Fig. 14 shows the experimental results for 8 drivers. The 8 drivers had different breathing rates, with the lowest breathing rate as 12 bpm, and the highest as 31 bpm. There were some differences in the test results of different people. But for all the cases, the errors in diver's breath rates were no more than 0.5 bpm, and the correlation coefficient was no less than 85%. Again the performances of the proposed Huber Kalman filter were better than the Kalman filter and the bandpass filter.

4) Impact of Multiple Passengers: We separately tested the impact on driver breath detection with different numbers of passengers in the car. The cases of 1-5 passengers were tested. As shown in Fig. 15, regardless of the number of passengers, the error of the respiration rate after the Huber Kalman filter is smaller than those after the bandpass filter and the Kalman filter. Passengers in other locations have little effect on the driver's breath detection. This is because the antenna is mounted behind the driver's seat. The antennas radiate forward, and any objects in the car along the other directions do not affect the driver's breathing detection.

5) Result of Abnormal Breathing: Since driver's respiration detection aims at monitoring the breathing of the driver, it shall be effective for both normal and abnormal breathing. The drivers are asked to intentionally change their breathing patterns in three cases during driving, including breathing from normal to apnea, from normal to fast, and from normal to slow. The result is shown in Fig. 16. It can be observed that the estimated breathing waveforms from the Huber Kalman filter are the best compared

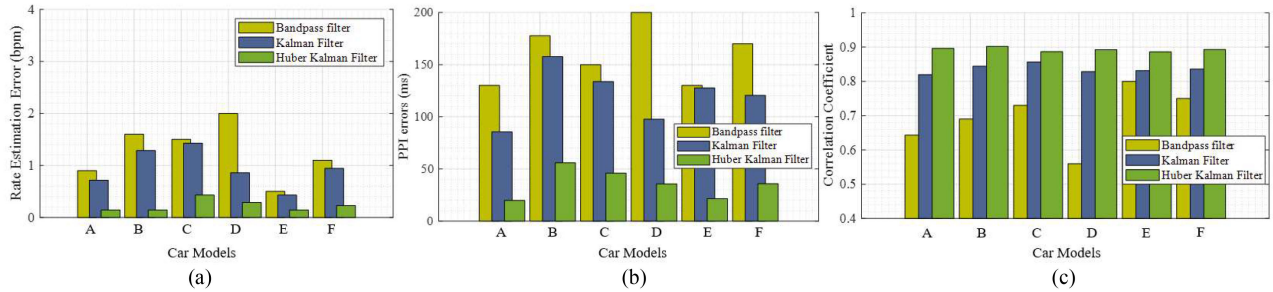

Fig. 13. Impact of different car models. (a) Breathing rate estimation error. (b) PPI errors. (c) Correlation coefficient.

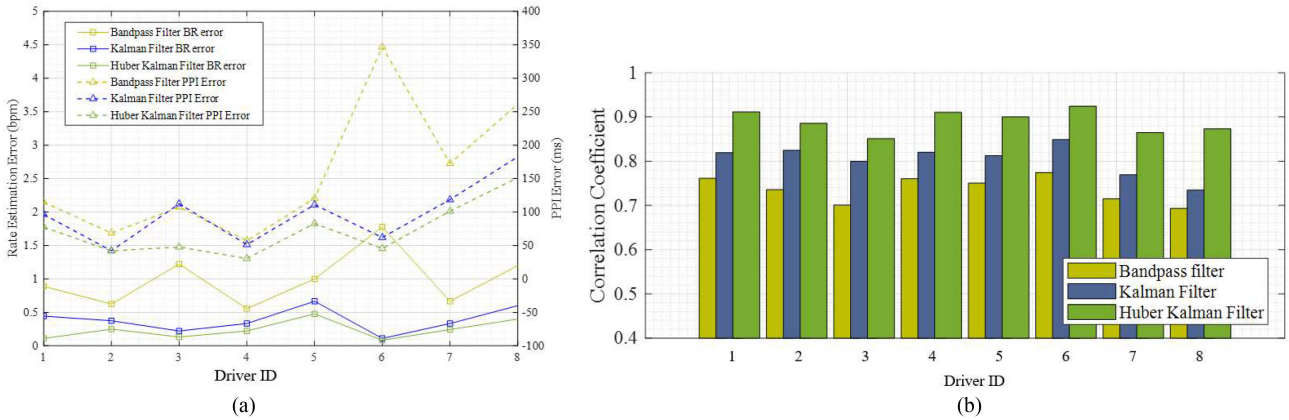

Fig. 14. Impact of different drivers. (a) Breathing rate estimation error and PPI errors. (b) Correlation coefficient.

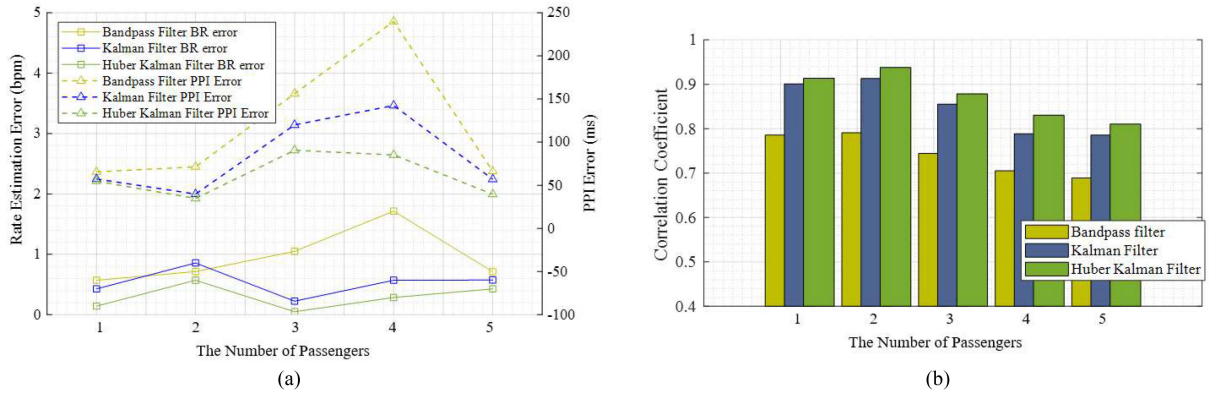

Fig. 15. Impact of multiple passengers. (a) Breathing rate estimation error and PPI errors. (b) Correlation coefficient.

to the actual breathing waveforms. As shown in Table II, the results of the Huber Kalman filter and the reference device maintain a strong correlation. With PPI detection, an abnormal respiration can be captured after a full cycle. And the detailed information that the rate of respiration increases or decreases is thus known.

V. Summary and Discussion

For the Wi-Fi based vital sign detection systems applied in the vehicle environment, the noise in the sensing data is complicated due to various road and driving conditions. Thus, effective noise filtering techniques are necessary. Compared with the conventional Kalman filter that is suitable for wireless sensing in static applications, the proposed Huber Kalman filter is more suitable for the moving objects under sensing, such as in the vehicular environments. Digital signal processing is an important part of wireless intelligent sensing (WISe) [32]. The proposed filtering method can provide low noise data for future data analytics for detailed driver health condition monitoring. The respiration waveform can be better extracted through the Huber Kalman filter, which is beneficial to the follow-up research on the relationship between respiration waveform and driving fatigue, as well as the relationship between PPI and fatigue. At the same time, heart rate and heart rate variability are also important and meaningful information for driver. In the future, we will also focus on the accurate extraction of the driver's heartbeat signal. We will analyze the characteristics of the driver's heart rate and

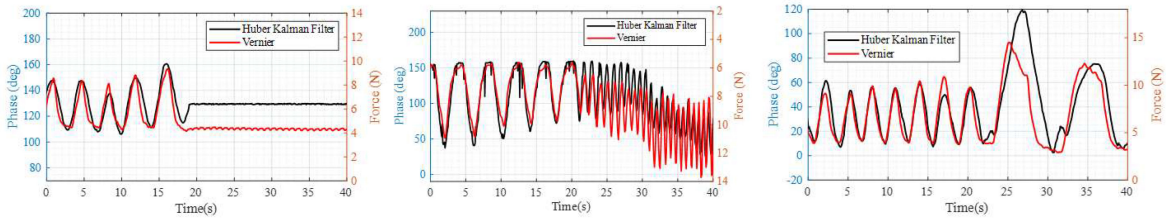

Fig. 16. Breathing waveform estimation in abnormal transitions. (a) From normal to apnea. (b) From normal to fast. (c) From normal to slow.

TABLE II
THE RESULT IN ABNORMAL TRANSITIONS

Abnormal Transitions	Methods	Breath Rate Errors (bpm)	PPI Errors (ms)	Corr-Coeff
Normal to Apnea	Bandpass	5	545	0.681
	KF	2	93	0.744
	HKF	0	78	0.892
Normal to Fast	Bandpass	4	287	0.709
	KF	1	116	0.867
	HKF	0	34	0.923
Normal to Slow	Bandpass	1	267	0.713
	KF	1	174	0.833
	HKF	0	84	0.877

heart rate variability to provide more data for driving safety. The proposed method in this paper can also be used for general robust data processing.

REFERENCES

[1] *Road Traffic Injuries*, Geneva, Switzerland: World Health Organization, 2019.

[2] C. Yang, X. Wang, and S. Mao, "Respiration monitoring with RFID in driving environments," *IEEE J. Sel. Areas Commun.*, vol. 39, no. 2, pp. 500–512, Feb. 2021.

[3] B. Warwick, N. Symons, X. Chen, and K. Xiong, "Detecting driver drowsiness using wireless wearables," in *Proc. IEEE 12th Int. Conf. Mobile Ad Hoc Sensor Syst.*, 2015, pp. 585–588.

[4] F. G. Fernández, M. F. Chimeno, and J. R. Castro, "Driver drowsiness detection based on respiratory signal analysis," *IEEE Access*, vol. 7, pp. 81826–81838, 2019.

[5] M. Rahman and B. I. Morshed, "Estimation of respiration rate using an inertial measurement unit placed on thorax-abdomen," in *Proc. IEEE Int. Conf. Electro Inf. Technol.*, 2021, pp. 1–5.

[6] X. Xu *et al.*, "BreathListener: Fine-grained breathing monitoring in driving environments utilizing acoustic signals," in *Proc. 17th Annu. Int. Conf. Mobile Syst., Appl., Serv.*, 2019, pp. 54–66.

[7] M. Kumar, A. Veeraraghavan, and A. Sabharwal, "DistancePPG: Robust non-contact vital signs monitoring using a camera," *Biomed. Opt. Exp.*, vol. 6, no. 5, pp. 1565–1588, 2015.

[8] J. Solaz *et al.*, "Drowsiness detection based on the analysis of breathing rate obtained from real-time image recognition," *Transp. Res. Procedia*, vol. 14, pp. 3867–3876, Apr. 2016.

[9] A. Singh, S. U. Rehman, S. Yongchareon, and P. H. J. Chong, "Multi-resident non-contact vital sign monitoring using radar: A review," *IEEE Sensors J.*, vol. 21, no. 4, pp. 4061–4084, Feb. 2021.

[10] F. Adib *et al.*, "Smart homes that monitor breathing and heart rate,"in *Proc. 33rd Annu. ACM Conf. Hum. Factors Comput. Syst.*, 2015, pp. 837–846.

[11] Y. Xiong, Z. Peng, C. Gu, S. Li, D. Wang, and W. Zhang, "Differential enhancement method for robust and accurate heart rate monitoring via microwave vital sign sensing," *IEEE Trans. Instrum. Meas.*, vol. 69, no. 9, pp. 7108–7118, Sep. 2020.

[12] J. Wang, X. Zhang, Q. Gao, H. Yue, and H. Wang, "Device-free wireless localization and activity recognition: A deep learning approach," *IEEE Trans. Veh. Technol.*, vol. 66, no. 7, pp. 6258–6267, Jul. 2017.

[13] X. Wang, C. Yang, and S. Mao, "PhaseBeat: Exploiting CSI phase data for vital sign monitoring with commodity WiFi devices," in *Proc. IEEE Int. Conf. Distrib. Comput. Syst.*, 2017, pp. 1230–1239.

[14] Q. Gao, J. Tong, J. Wang, Z. Ran, and M. Pan, "Device-free multi-person respiration monitoring using WiFi," *IEEE Trans. Veh. Technol.*, vol. 69, no. 11, pp. 14083–14087, Nov. 2020.

[15] J. Liu, Y. Chen, Y. Wang, X. Chen, J. Cheng, and J. Yang, "Monitoring vital signs and postures during sleep using WiFi signals," *IEEE Internet Things J,* vol. 5, no. 3, pp. 2071–2084, Jun. 2018.

[16] X. Wang, C. Yang, and S. Mao, "TensorBeat: Tensor decomposition for monitoring multi-person breathing beats with commodity WiFi," *ACM Trans. Intell. Syst. Technol.*, vol. 9, no. 1, pp. 1–27, Sep. 2017.

[17] X. Liu, J. Cao, S. Tang, J. Wen, and P. Guo, "Contactless respiration monitoring via off-the-shelf WiFi devices," *IEEE Trans. Mobile Comput.,* vol. 15, no. 10, pp. 2466–2479, Oct. 2016.

[18] J. Wang, J. Tong, X. Fan, X. Ma, Q. Gao, and X. Huang, "A dynamic differential phase analysis method for wireless sensing," *IEEE Trans. Veh. Technol.,* vol. 68, no. 8, pp. 7723–7732, Aug. 2019.

[19] M. Hussain, A. Akbilek, F. Pfeiffer, and B. Napholz, "In-vehicle breathing rate monitoring based on WiFi signals," in *Proc. 50th Eur. Microw. Conf.*, 2021, pp. 292–295.

[20] S. D. D. Cruz, H. Beise, U. Schröder, and U. Karahasanovic, "A theoretical investigation of the detection of vital signs in presence of car vibrations and RADAR-based passenger classification," *IEEE Trans. Veh. Technol.*, vol. 68, no. 4, pp. 3374–3385, Apr. 2019.

[21] F. Schadt and F. Mohr, "Application of Kalman filters as a tool for phase and frequency demodulation of IQ signals," in *Proc. IEEE Region 8 Int. Conf. Comput. Technol. Elect. Electron. Eng.*, 2008, pp. 421–424.

[22] R. E. Kalman, "A new approach to linear filtering and prediction problems," *J. Build. Eng.*, vol. 82, no. 1, pp. 35–45, Mar. 1960.

[23] F. Farahi and H. S. Yazdi, "Probabilistic Kalman filter for moving object tracking," *Signal Process. Image Commun.*, vol. 82, no. 1, pp. 115751–115761, Mar. 2020.

[24] M. Jonasson, Å. Rogenfelt, C. Lanfelt, J. Fredriksson, and M. Hassel, "Inertial navigation and position uncertainty during a blind safe stop of an autonomous vehicle," *IEEE Trans. Veh. Technol.*, vol. 69, no. 5, pp. 4788–4802, May 2020.

[25] J. W. Bandler, S. H. Chen, R. M. Biernacki, L. Gao, K. Madsen, and H. Yu, "Huber optimization of circuits: A robust approach," *IEEE Trans. Microw. Theory Techn.*, vol. 41, no. 12, pp. 2279–2287, Dec. 1993.

[26] S. Lee, Y. D. Park, Y. J. Suh, and S. Jeon, "Design and implementation of monitoring system for breathing and heart rate pattern using WiFi signals," in *Proc. 15th IEEE Annu. Consum. Commun. Netw. Conf.*, 2018, pp. 1–7.

[27] X. Liu, J. Cao, S. Tang, and J. Wen, "Wi-sleep: Contactless sleep monitoring via WiFi signals," in *Proc. IEEE Real-Time Syst. Symp.*, 2014, pp. 346–355.

[28] J. C. Lagarias, J. Cao, S. Tang, and J. Wen, "Convergence properties of the Nelder–Mead simplex method in low dimensions," in *Proc. IEEE Real-Time Syst. Symp.*, 1998, pp. 112–147.

[29] Y. Wang, W. Wang, M. Zhou, A. Ren, and Z. Tian, "Remote monitoring of human vital signs based on 77-GHz mm-wave FMCW radar," *IEEE Sensors J.*, vol. 20, no. 10, May 2020, Art. no. 2999.

[30] P. Hamelmann, R. Vullings, M. Mischi, A. F. Kolen, L. Schmitt, and J. W. M. Bergmans, "An extended Kalman filter for fetal heart location estimation during Doppler-based heart rate monitoring," *IEEE Trans. Instrum. Meas.*, vol. 68, no. 9, pp. 3221–3231, Sep. 2019.

[31] R. J. Meinhold and N. D. Singpurwalla. "Understanding the Kalman filter," *J. Amer. Stat. Assoc.*, vol. 37, no. 2, pp. 123–127, May. 1983.

[32] A. Qi *et al.*, "WISe: Wireless intelligent sensing for human-centric applications," *IEEE Wireless Commun.*, to be published, doi: 10.1109/MWC.012.2100656.

Yang Yang (Student Member, IEEE) received the B.E. degree in communication engineering in 2020 from Southwest Jiaotong University, Chengdu, China, where she is currently working toward the M.E. degree in information and communication engineering. Her research interests include wireless sensing and signal processing.

Yunlong Luo (Student Member, IEEE) received the B.E. and M.E. degrees in electronic engineering from Hunan University, Changsha, China, in 2016 and 2019, respectively. He is currently working toward the Ph.D. degree in information and communication engineering, Southwest Jiaotong University, Chengdu, China. His research interests include high precision positioning, hardware system design, and wireless sensing. He is involved in the research and development of Pontosense and Mercku. Mercku has won several CES awards, including the CES Wellness Product Of The Year Award (2022), CES Networking Product Of The Year Award (2021), CES Innovation Award honoree (2020, 2019), he is one of the key Technical Leaders for these awards.

Alex Qi (Member, IEEE) received the BMATH from the University of Waterloo, Waterloo, ON, Canada, the B.B.A. degree from Wilfrid Laurier University, Waterloo, and the M.B.A. degree from The University of Chicago Booth School of Business, Chicago, IL, USA. He is currently a Technology Professional focusing on markets related to wireless communications, smart homes, and the Internet of Things. He is the Co-founder and CEO of Pontosense, a leading communications company focused on innovative home products and applications. Mercku's Red Dot award-winning, second-generation mesh Wi-Fi system currently sells in more than 45 countries worldwide. Over the past year, Mercku has innovated into wireless sensing, enabling vital sign measurement without wearables, empowering new features for the automotive and smart home industries. Formerly, he was a management consultant for Kearney.

Ge Shi (Member, IEEE) received the B.S. degree in measurement, control technology, and instruments from Tsinghua University, Beijing, China, in 2007, and the M.S. degree in mechanical science and engineering from the University of Illinois at Urbana Champaign, Champaign, IL, USA, in 2009. His research interests include research and development of wireless communication and wireless sensing technology.

Miao Miao (Member, IEEE) received the M.S. degree in computer science and economics from the University of Science & Technology Beijing, Beijing, China, in 2004, and the Ph.D. degree in computer science and economics from Southwest Jiaotong University, Chengdu, China, in 2007. During 2007–2021, she was a Professor with the School of Economics and Management, Southwest Jiaotong University. She is currrently with Yango University, Myanmar, and is also the Vice-President of the School of Economics and Management. Her research interests include e-commerce, user behavior modeling, and IoT systems.

Jun Fan (Fellow, IEEE) received the B.S. and M.S. degrees in electrical engineering from Tsinghua University, Beijing, China, in 1994 and 1997, respectively, and the Ph.D. degree in electrical engineering from the University of Missouri-Rolla, Rolla, MO, USA, in 2000. From 2000 to 2007, he was a Consultant Engineer with NCR Corporation, San Diego, CA, USA. In July 2007, he was with the Missouri University of Science and Technology (formerly University of Missouri-Rolla), where he is currently an Associate Professor with Missouri Science and Technology Electromagnetic Compatibility (EMC) Laboratory. His current research interests include signal integrity and EMI designs in high-speed digital systems, dc power-bus modeling, intra-system EMI and RF interference, PCB noise reduction, differential signaling, and cable/connector designs. Dr. Fan was the Chair of the IEEE EMC Society TC-9 Computational Electromagnetics Committee from 2006 to 2008 and was a Distinguished Lecturer of the IEEE EMC Society in 2007 and 2008. He is currently the Vice Chair of the Technical Advisory Committee of the IEEE EMC Society and an Associate Editor for IEEE TRANSACTIONS ON ELECTROMAGNETIC COMPATIBILITY and the *EMC Magazine*. He was the recipient of the IEEE EMC Society Technical Achievement Award in August 2009.

Jianhua Ma (Senior Member, IEEE) is currently a Professor with the Faculty of Computer and Information Sciences, Hosei University, Tokyo, Japan. From 2011 to 2012, he was the Chair of Digital Media Department, Hosei University, Tokyo, Japan. He has authored or coauthored more than 300 papers, coauthored/edited more than 15 books and 30 journal special issues. His research interests include multimedia, networking, pervasive computing, social computing, wearable technology, IoT, smart things, and cyber intelligence. He is the Chair of IEEE SC Hyper-Intelligence Technical Committee, the Co-chair of IEEE SMC Technical Committee on Cybermatics, and a Founder of IEEE CIS Technical Committee on Smart World.

Yihong Qi (Senior Member, IEEE) received the Ph.D. degree from Xidian University, Xi'an, China, in 1989. He is currently the CTO of Pontosense. He is an Honorary Professor with Xidian University and Southwest Jiaotong University, Chengdu, China. He is also an Adjunct Professor with the EMC Laboratory, Missouri University of Science and Technology, Rolla, MO, USA, Western University, London, ON, Canada, Hunan University, Changsha, China, Dalian Maritime University, Dalian, China, and Southwest University of Science and Technology, Mianyang, China. He is an Inventor of 500 published and pending patents. From 1995 to 2010, he was with Research in Motion (Blackberry), Waterloo, ON, Canada, where he was the Director of Advanced Electromagnetic Research. He is the Founder of five technology companies.

Dr. Qi was a Distinguished Lecturer of IEEE EMC Society, and the founding Chairman of the IEEE EMC TC-12. He was the recipient of the IEEE EMC Society Technical Achievement Award, CES Innovation Award 2019 and 2020, Network Product of the year in Award 2021 and Wellness Product of the Year Award 2022. He is an Associate Editor for the IEEE INTERNET OF THINGS JOURNAL and IEEE TRANSACTIONS ON ELECTROMAGNETIC COMPATIBILITY. He is a Fellow of Canadian Academy of Engineering and Fellow of National Academy of Inventors.